The Effect of Long-Term Thermal Exposure on the Microstructure and Stress Rupture Property of a Directionally Solidified Ni-Based Superalloy

X.W. JIANG, D. WANG, G. XIE, H. LI, L.H. LOU, and J. ZHANG

Microstructural degradation and microstructure-property relationship during long-term thermal exposure in a directionally solidified Ni-based superalloy are systematically studied. The coarsening kinetics of γ' precipitation conforms well to the LSW model during the long-term thermal exposure. The detailed time dependence of MC decomposition during the long-term thermal exposure is revealed. Grain boundary coarsening was mainly facilitated by γ' and $M_{23}C_6$ precipitates coarsening in GBs region, and the GB coarsening kinetics conforms well to the JMAK theory. During different stages of the thermal exposure, dominant factors for the decrease of stress-rupture lifetime vary due to the evolution of multiple microstructures (γ' coarsening, MC decomposition, and grain boundary coarsening).

DOI: 10.1007/s11661-014-2559-8

I. INTRODUCTION

THE materials applied in industrial gas turbine blades are expected to withstand high temperature and stress during long-term service. It is reported that the proper examining and repairing interval of gas turbine blades is 24,000 equivalent operation hours (EOH) and the total service life is beyond 50,000 EOH.[1,2] Extensive studies have shown that prolonged thermal and stress exposure causes multiple microstructural degradations such as γ' coarsening and rafting, MC carbides decomposition, secondary precipitations along grain boundaries, and formation of TCP phases and cavity or void in the gas turbine blades after long-term service, almost all of which are detrimental to mechanical properties.[3–5]

The morphologies and mechanisms associated with γ' particle coarsening upon aging have been a topic of significant discussion over the past decades.[6–10] Since the changes in morphology, size, and distribution of γ' precipitates during long-term thermal exposure mainly cause the degradation of tensile strength and creep resistance, it is very important to monitor the evolution of γ', be able to predict the kinetics of growth during long-term thermal exposure, and correlate that with mechanical properties. However, the evolution of size/morphology and volume fraction of γ' precipitates during long-term thermal exposure beyond 20,000 hours and its impact on the creep properties of superalloys have been seldom reported in previous studies.

Compared to single crystal (SC) Ni-based superalloys, directional solidification (DS) Ni-based superalloys have a particular creep deformation characteristic due to MC decomposition in grain boundary (GB) region and grain boundary precipitates coarsening during long-term thermal exposure. Unfortunately, limited information is available for the coarsening kinetics of grain boundaries and the effects on creep property of DS Ni-based superalloys during long-term thermal exposure.

It is interesting to note that most of the above microstructural evolutions are reversible, in the sense that they can be rejuvenated by re-heat treatment and hot isostatic pressing (HIP).[11,12] Unfortunately, primary MC decomposition is irreversible and may affect the microstructure stability and mechanical properties of the rejuvenated blades during the next service cycle.[4,11–13] Three classical reactions, $MC + \gamma \rightarrow M_{23}C_6 + \gamma'$, $MC + \gamma \rightarrow M_{23}C_6 + \eta$, and $MC + \gamma \rightarrow M_{23}C_6 + (MC)_{deg}$, are often operative in the alloys, such as GTD-111 and In-738 applied in industrial gas turbine blades after long-term thermal and stress exposure.[3–5,14] The mechanism of primary MC decomposition in gas turbine blades made from both conventionally cast (CC) superalloys and directionally solidified (DS) alloys was reported in these previous studies.[3–5] However, there is not much published information on the time dependence of MC decomposition in terms of morphological and compositional evolution during long-term thermal exposure. Moreover, there is still augment regarding the role of MC carbides decomposition during creep after long-term thermal exposure. Some researchers thought that MC carbides decomposed into fine $M_{23}C_6$ particles, which played a positive role in influencing the long-term creep rupture properties of the DS superalloys,[15–18] whereas others insisted that MC decomposition provided the site

X.W. JIANG, Ph.D. Candidate, D. WANG, Assistant Researcher, G. XIE, Associate Researcher, and H. LI and L.H. LOU, Professors, are with the Superalloys Division, Institute of Metal Research, Chinese Academy of Sciences, 72 Wenhua Road, Shenyang 110016, P. R. China. Contact e-mail: dwang@imr.ac.cn J. ZHANG, Professor, is with the Superalloys Division, Institute of Metal Research, Chinese Academy of Sciences, and also with the Shenyang National Laboratory for Materials Science, Institute of Metal Research, Chinese Academy of Sciences, 72 Wenhua Road, Shenyang 110016, P.R. China.

Manuscript submitted March 4, 2014.
Article published online September 17, 2014

of cracks initiation, which was deleterious and contributed to the failure of creep specimens.[5,19,20]

Obviously, during long-term thermal exposure, the mechanical performance of superalloys is closely related to the microstructural degradations. However, the effect of multiple microstructural degradations (*e.g.*, γ' coarsening, MC decomposition, and secondary precipitations coarsening along GBs) on mechanical properties of DS Ni-based superalloys during different stages of thermal exposure has seldom been reported in previous studies. In this paper, we studied the evolution of microstructure as well as the creep rupture properties during long-term thermal exposure. The relationships between microstructural evolution and stress rupture properties of the DS Ni-based superalloy have been correlated as a first attempt to explore the possible life assessment methodology.

II. EXPERIMENTAL

The nickel-based superalloy DZ411 in our present study is a typical hot corrosion resistant alloy applied in industrial gas turbine blades with 14.2Cr, 9.5Co, 3.1Al, 5.0Ti, 3.0Ta, 3.6W, 1.5Mo, with 0.1C and 0.01B, and balance Ni, in weight percent. The cylindrical specimens with the size of Φ16 mm × 220 mm were DS by the conventional Bridgman process. The specimens received the standard solution and age heat treatment, 1493 K (1220 °C)/2 hours/air cooling (AC), 1393 K (1120 °C)/2 hours/AC, and 1123 K (850 °C)/24 hours/AC. Then the as-heat-treated specimens were subjected to a long-term thermal exposure at 1173 K (900 °C) up to 24,000 hours. The thermally exposed specimens were machined into creep specimens in the longitudinal direction with gage length of 25 mm and a gage diameter of 5 mm to test the creep rupture property at 1253 K (980 °C) and 220 MPa.

Specimens after different periods of thermal exposure were cut and prepared by standard procedure for microstructural observations, *i.e.*, they were polished and either etched electrolytically with a solution of 10 mL H_3PO_4 + 90 mL H_2O under a voltage of 7 to 10 V for 10 seconds mainly for the microstructural examination of γ' precipitates or etched chemically with a solution of 17 mL HNO_3 + 100 mL HCl + 7.5 g $CuCl_2$ + 7.5 g $FeCl_3$ mainly for the microstructural examination of MC and $M_{23}C_6$ carbides. The microstructural examination of γ' precipitation was performed using a scanning electron microscopy (SEM). Backscattered electron (BSE) imaging was used to observe the microstructure of MC and $M_{23}C_6$ carbides. Chemical composition of carbides was analyzed by electron probe micro-analyzer (EPMA). Size (equivalent diameter) and volume fraction of the γ' particles were characterized on the SEM micrographs using Image Tool software. The equivalent diameter is defined as the diameter of a circle with an equal area of a feature of arbitrary shape. In order to evaluate average area fraction and equivalent diameter, more than 10 SEM micrographs were recorded from different areas for each sample, and 50 γ' particles per micrograph were considered. The width of grain boundaries was characterized by measuring the average thickness of GB wrapped by γ' precipitates and $M_{23}C_6$ carbides in the transverse direction of the specimens.

III. RESULTS

A. *Microstructure After Heat Treatment*

The primary dendrite arm spacing of the as-cast samples is around 250 μm. Microstructure of the alloy after heat treatment was mainly composed of γ matrix, γ' precipitates, residual γ/γ' eutectics, and primary MC carbides within grain interiors (GIs) and along grain boundaries (GBs), as shown in Figure 1. The secondary γ' precipitates were cubic, and the average size and area fraction were about 0.4 μm and 54 pct respectively. Numerous hyperfine tertiary γ' precipitates forming during the aging treatment could be observed in the matrix channel (Figure 1(b)). The volume fraction of residual γ/γ' eutectics was less than 1.5 pct. Primary MC carbides as block were scattered within grain interiors as well as along grain boundaries (Figure 1(c)). Chemical composition of primary MC carbides in the heat-treated alloy measured by EPMA is illustrated in Table I. It can be seen that, the main elements forming primary MC carbides are Ti, Ta, and W. γ' precipitates along grain boundaries were cubic and the size was about 0.6 μm (Figure 1(d)).

B. *Microstructural Degradation During Long-Term Thermal Exposure*

During long-term thermal exposure at 1173 K (900 °C), the microstructure of the experimental alloy degenerates gradually, which depends on the aging time. Figures 2 through 6 show the typical microstructure evolution of γ', primary MC carbides, and grain boundaries during the long-term thermal exposure.

1. *Evolution of γ' precipitates*

A significant change of morphology, size, and area fraction of γ' precipitates can be found during long-term thermal exposure at 1173 K (900 °C). In the specimen exposed for 5000 hours, tertiary γ' precipitates dissolved and the secondary γ' particles became larger and degenerated to the cube morphology with rounded corner, which widens the matrix spacing between the γ' precipitates (Figure 2(a)). Coarsening process of secondary γ' precipitation was going on as the thermal exposure was prolonged to 9000 hours (Figure 3(a)). As the thermal exposure was over 15,000 hours, the large irregular plate morphology of γ' precipitation was present over the entire sample due to the growth and coalescence of smaller γ' precipitates (Figures 4(a) through 6(a)). As shown in Figure 7, size (equivalent diameter) of secondary γ' precipitates increased gradually, and there was a tiny change to be seen for area fraction of secondary γ' with the increasing aging time.

2. *Decomposition of primary MC carbides*

Primary MC carbides remained stable and only dissolved at the edge within the first 5000 hours exposure as seen in Figures 2(b) and (c). Similar to the

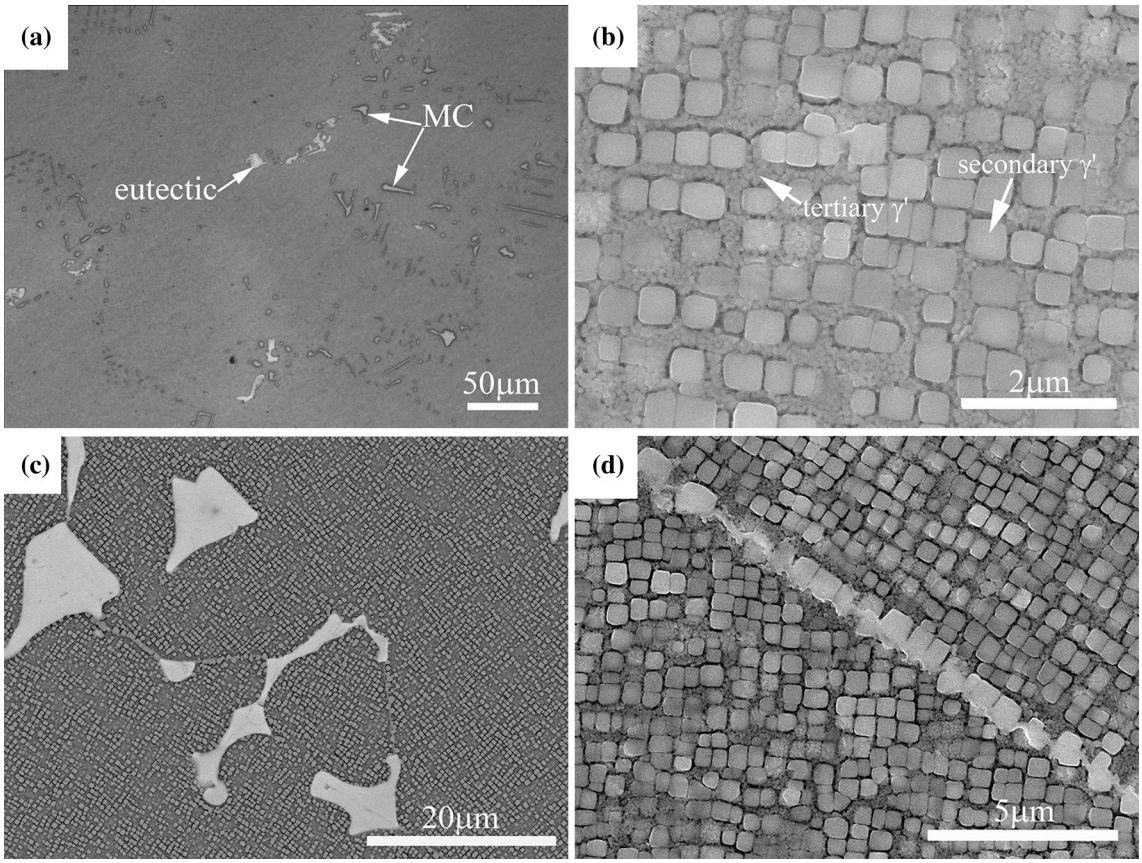

Fig. 1—Microstructure of the as-heat-treated alloy: (*a*) residual γ/γ' eutectics and MC carbides, (*b*) γ' precipitates, (*c*) primary MC carbides within GIs and along GBs, and (*d*) γ' precipitates at grain boundary.

Table I. Chemical Composition of Primary MC Carbides in the As-Heat-Treated Alloy

Element	Ti	Cr	Ni	Mo	Co	Ta	W	C
Wt pct	25.899	0.632	2.702	0.359	0.498	55.470	4.734	9.706
At. pct	30.871	0.694	2.628	0.213	0.483	17.503	1.470	46.137

previous observation,[3–5] a thin well-defined decomposition zone was also observed on the peripheries of primary MC carbides both within GIs and along GBs as seen in Figure 2(b). As is reported,[3–5] the chemical composition at the decomposition zone is consistent with that of MC carbides, with part of the Ti and Ta atoms replaced by Ni, Co, and Cr.

As the thermal exposure was extended to 9000 and 15,000 hours, fine gray particles were found in the vicinity of primary MC within GIs as well as at grain boundaries (Figures 3(b) and (c)). The discrete gray particles were identified by EDS as $M_{23}C_6$ carbides with high Cr content (Figure 3(e)).

As the thermal exposure was prolonged to 20,000 and 24,000 hours, MC decomposition proceeded and more coarsened $M_{23}C_6$ particles precipitated within GIs as well as at GBs, as shown in Figures 5 and 6. In addition, the $M_{23}C_6$ particles were wrapped by γ' as illustrated in Figure 6(d). Similar to the classical reaction,[5] the decomposition of primary MC can be summarized as $MC + \gamma \rightarrow M_{23}C_6 + \gamma'$. Meanwhile, more decomposed MC began to break down into disintegrated MC fragments (<2 μm) with the extended aging time, as indicated by the black arrow in Figure 5(b), and variations of the percentage of primary MC carbides showing disintegration *vs* aging time both within GIs and at GBs are shown in Figure 8. Moreover, it should also be noted that primary MC carbides located at or near the GBs exhibited a higher degree of decomposition than those in the GIs.

3. *Grain boundary evolution*

Discrete $M_{23}C_6$ particles wrapped by γ' precipitated along GB within the first 5000 hours at 1173 K (900 °C) as shown in Figures 2(c) and (d). As the thermal exposure was prolonged up to 24,000 hours, $M_{23}C_6$ particles wrapped by γ' in grain boundaries region continued to coarsen and merged with each other, and consequently, resulted in the formation of a continuous layer of $M_{23}C_6$ and γ' precipitates (Figure 6). The width

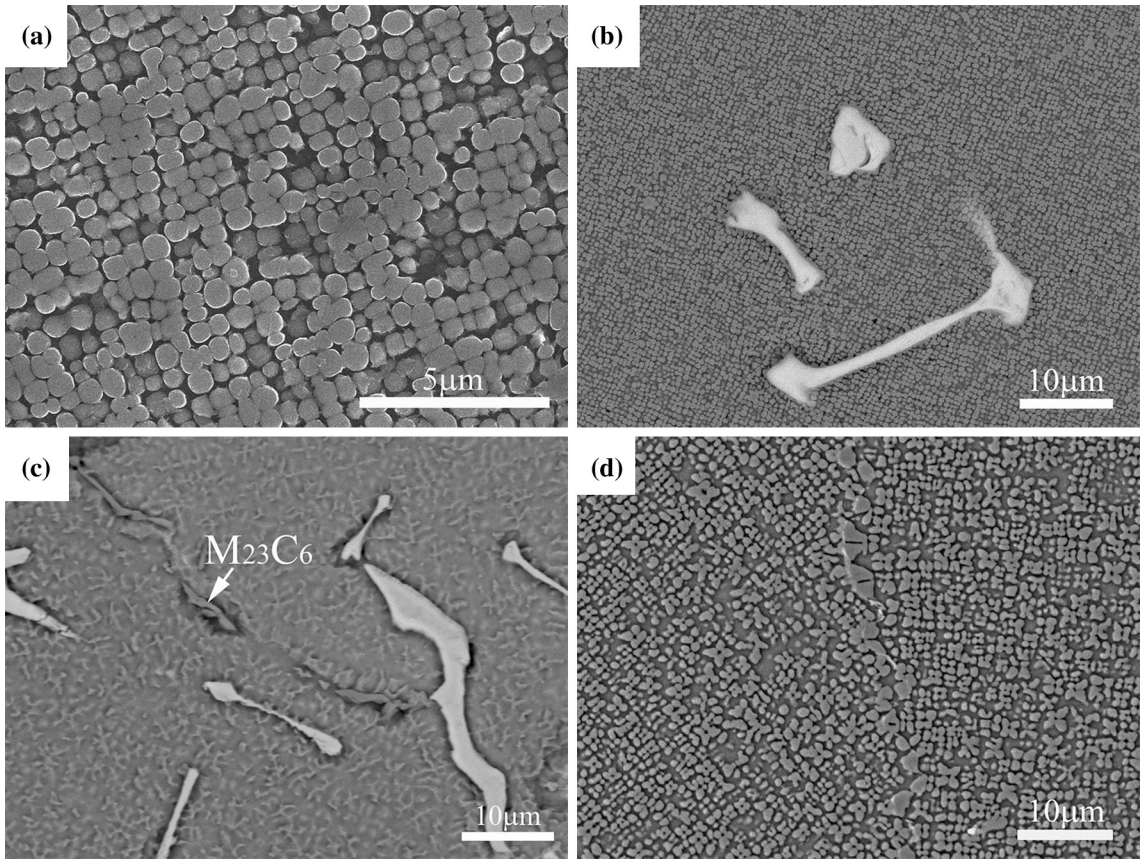

Fig. 2—Microstructure in the thermally exposed alloy for 5000 hours: γ' precipitates (*a*) and primary MC carbides within GIs (*b*) and along GBs (*c*) and γ' precipitates at grain boundary (*d*).

of the $M_{23}C_6$ and γ' layer at GBs during thermal exposure is shown in Figure 9. It can be seen that the coarsening rate of GB increases within the first 10,000 hours and then slows down during further exposure.

C. *Degradation of Stress Rupture Property*

The stress-rupture lifetime of the thermally exposed specimens at 1253 K (980 °C) reduces remarkably with the extended thermal exposure, and the elongation increased from 16 to 31 pct within 5000 hours exposure and then decreased to 23 pct up to 24,000 hours, as illustrated in Figures 10(a) through (b). The evolution of stress-rupture lifetime can be divided into three stages. The stress-rupture lifetime decreases sharply by 50 pct within 5000 hours and then remains at a steady level from 5000 to 15,000 hours. Finally, the lifetime of stress rupture decreases drastically again to about 20 hours as the thermal exposure time is over 20,000 hours.

The microstructure of longitudinal section near the rupture site of the thermally exposed specimens for 5000 and 24,000 hours is shown in Figure 11. Compared to the thermally exposed specimens within 5000 hours, more microcracks in the thermally exposed specimen for 24,000 hours were observed near the rupture site (Figures 11(a) and (b)). It is clearly shown that numerous microcracks initiated and grew in the position of curve GBs (Figure 11(c)), where decomposed MC and coarsened $M_{23}C_6$ and γ' precipitated after 24,000 hours of thermal exposure (Figure 11(d)).

IV. DISCUSSION

A. *Microstructural Degradation During Long-Term Thermal Exposure*

1. γ' *evolution*

In some alloys, the time-dependent γ' coarsening process conforms to the LSW model:[6,7]

$$\bar{D}_t^3 - \bar{D}_0^3 = kt,$$

where $\bar{D}_t$ is the mean particle size at a time t, $\bar{D}_0$ is the mean particle size at the onset of coarsening ($t = 0$), and k is the coarsening rate constant.

Tertiary γ' precipitates dissolved during the thermal exposure at 1173 K (900 °C) within 5000 hours aging. With the thermal exposure prolonged, coarsening and coalescence of secondary γ' precipitates occurred, which is driven by the reduction in total interfacial energy. The variations of $\bar{D}_t^3 - \bar{D}_0^3$ *vs* time for secondary γ' precipitates are shown in Figure 12, according to our present experimental date shown in Figure 7. It is clear that the coarsening kinetic for the secondary γ' precipitates follows approximately a linear relation, which conforms well to the LSW theory.

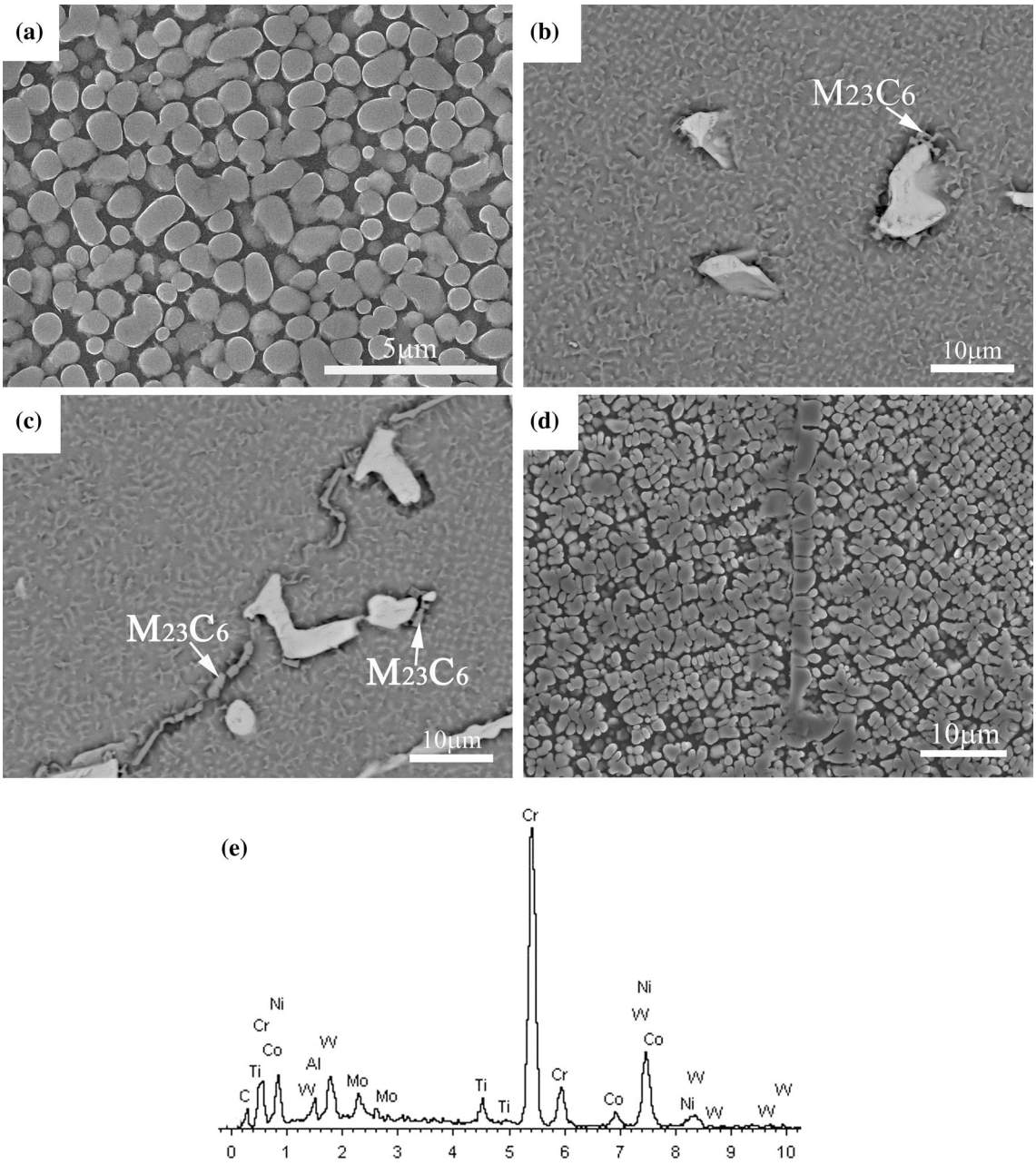

Fig. 3—Microstructure in the thermally exposed alloy for 9000 h: γ' precipitates (*a*); primary MC carbides within GIs (*b*) and along GBs (*c*); γ' precipitates at grain boundary (*d*); EDX spectra of the discrete gray particles on the periphery of primary MC (*e*).

2. *Carbides decomposition*

Compared to the primary MC carbides in the virgin alloy (Figure 1(c)), primary MC carbides in the thermally exposed alloy within 5000 hours were surrounded by a decomposed zone. During thermal exposure within 5000 hours, the primary MC carbides with high carbon content serve as a carbon resource and γ matrix as a Ni, Cr, and Co reservoir. Outward diffusion of carbon from the primary MC carbides into the surrounding matrix and inward diffusion of Ni, Cr, and Co from the γ matrix develop a well-defined transition zone around the primary MC carbides.[5] The replacement of the strong carbide forming atoms such as Ti, Ta, and W with Ni, Co, and Cr atoms resulting from the outward and inward diffusion is known to weaken the interatomic bonds in the primary MC carbides and results in the decrease of their stability and disintegration in the prolonged thermal exposure.[3]

With the thermal exposure extended over 9000 and 15,000 hours, primary MC carbides were subjected to further decomposition due to the enrichment of the elements of C and Cr through the outward and inward diffusion between MC and γ matrix, creating the favorable environment for the formation of $M_{23}C_6$ precipitations in the vicinity of the decomposed primary MC carbides.

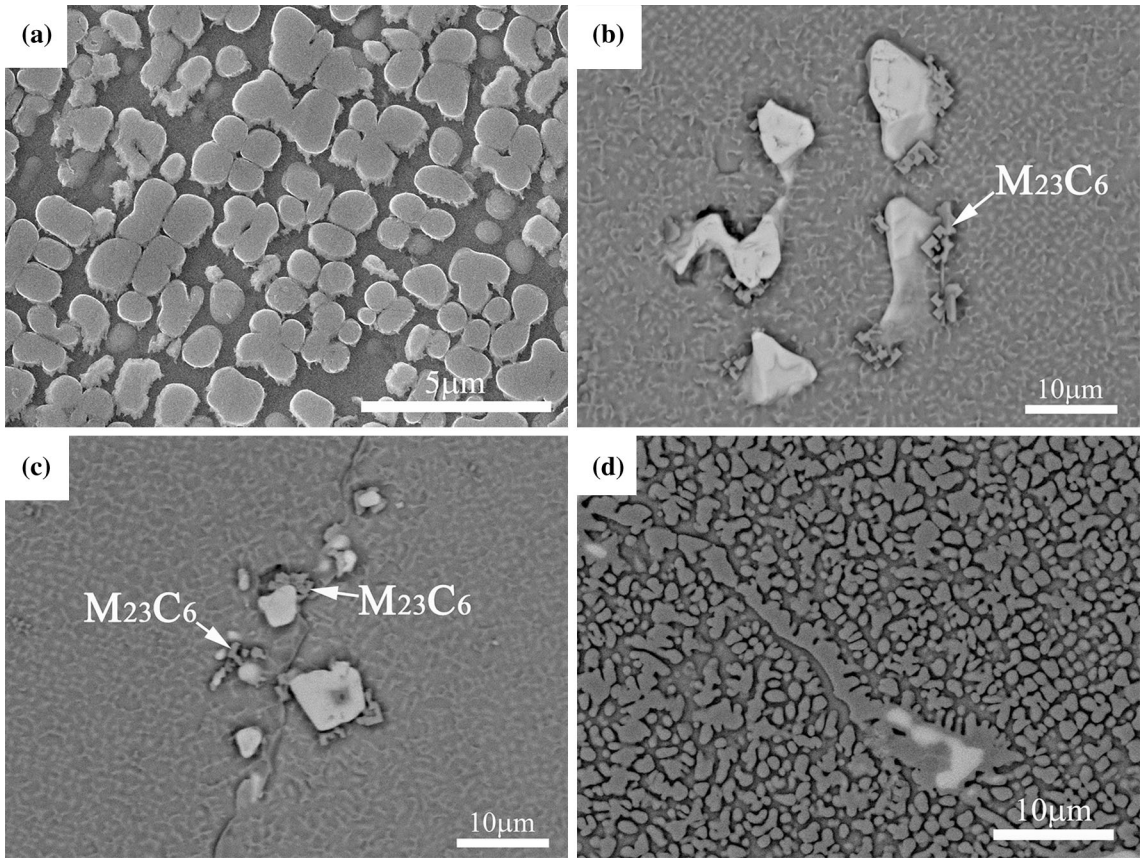

Fig. 4—Microstructure in the thermally exposed alloy for 15,000 h: γ' precipitates (*a*) and primary MC carbides within GIs (*b*) and along GBs (*c*) and γ' precipitates at grain boundary (*d*).

With the thermal exposure extended to 20,000 and 24,000 hours, the decomposition of primary MC carbides proceeded and more decomposed MC began to break up into disintegrated MC-type particles, especially in GB region. Moreover, the precipitations of $M_{23}C_6$ carbides along GBs resulted in the local enrichment with γ' forming elements, Al, Ti, and Ta, allowing γ' film to form along GBs.[21] It is obvious that primary MC carbides along GBs underwent a more severe decomposition than those within GIs due to faster diffusion and enrichment of elements such as C and Cr through the diffusion path along GBs, creating the favorable environment for severe disintegration of primary MC and the formation of considerable $M_{23}C_6$ precipitations. The disintegrated MC particles have a much higher surface/volume ratio than primary MC, and outward and inward element diffusion rate for the particles is considerably faster as compared to primary MC decomposition. Hence, the decomposition rate of the disintegrated MC particle might be faster than primary MC carbides during the extended thermal and stress exposure, and the related work will be done in the near future.

3. *Grain boundary (GB) evolution*

Grain boundary coarsening during long-term thermal exposure is mainly facilitated by $M_{23}C_6$ and γ' precipitates coarsening in the GBs region. GB energy is the main driving force of elements diffusion along GBs, which significantly influences $M_{23}C_6$ and γ' precipitates coarsening and MC degeneration along GBs during the long-term thermal exposure.

Different from the coarsening behavior of γ' precipitates within GIs *via* Ostwald ripening, GB coarsening is associated with directional coarsening and coalescence of $M_{23}C_6$ and γ' precipitates *via* faster GB diffusion, for which LSW theory can't be applied directly.[22] The Johnson–Mehl–Avrami–Kolmogorov (JMAK) theory has been applied to quantify microstructural evolution in isothermal situation.[22–25] The JMAK equation for an isothermal transformation can be written as[25]

$$f(t) = 1 - \exp(-kt^n),$$

where k is a constant and n is an integer or half integer. The variations of $\ln[-\ln(1-f(t))]$ *vs* $\ln t$ follow a linear line, according to the equation above. The variations of width of coarsened GB during long-term isothermal exposure can be described as[22]

$$f(t) = \frac{W_t - W_0}{W_f - W_0},$$

where W_t is the mean width of GB at a time t of the thermal exposure, W_0 is the mean width of GB at the

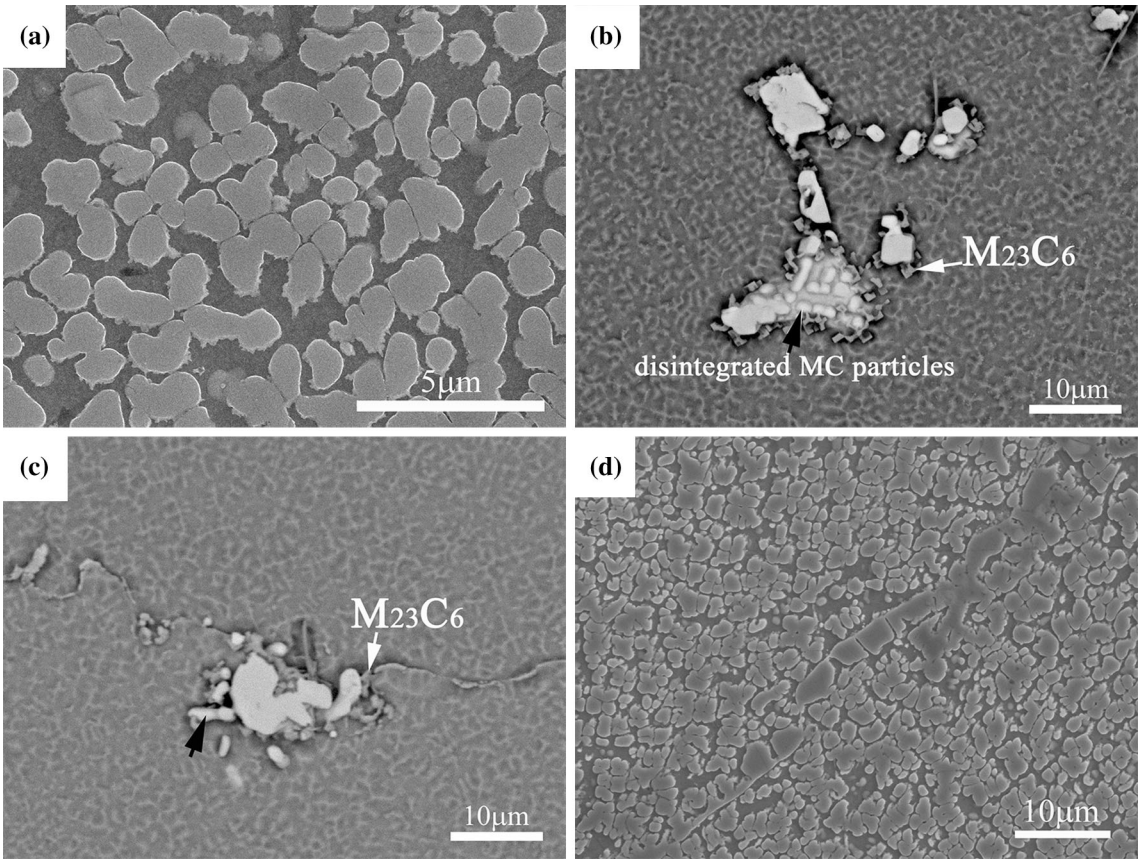

Fig. 5—Microstructure in the thermally exposed alloy for 20,000 h: γ' precipitates (*a*) and primary MC carbides within GIs (*b*) and along GBs (*c*) and γ' precipitates at grain boundary (*d*).

onset of the thermal exposure ($t = 0$ hours) and W_f is the mean width of GB at the final state of coarsening ($t = 24{,}000$ hours).

The variations of $\ln[-\ln(1-f(t))]$ *vs* $\ln t$ in our study are shown in Figure 13. The GB coarsening kinetic follows approximately a linear line, which conforms well to the JMAK theory.

B. *Influence of Microstructural Degradation on Stress Rupture Property*

The DS DZ411 nickel-based superalloy is strengthened primarily by γ' phase. The mechanical properties depend on the morphology, size, volume fraction, and distribution of the γ' precipitates.[26–30] Compared to γ' precipitates in the "new" alloy, hyperfine tertiary γ' precipitates disappear and secondary γ' precipitates degenerate to the cube morphology with rounded corner, which enlarges the spacing between the γ' precipitates after 5000 hours thermal exposure, and it is easier for the dislocations to move in the γ matrix. Moreover, it has been reported that when the size of γ' precipitates ranges from approximately 0.5 to 0.8 μm (approaching to the evolution of γ' precipitates between 0 and 5000 hours thermal exposure), the creep life is inversely proportional to the size of γ' precipitates.[30] Moreover, the initial GB coarsening and stable primary MC carbides within 5000 hours are generally considered to have a negligible influence on the initiation and propagation of microcracks, as illustrated in Figure 11(a). Therefore, a significant decrease of stress rupture life of the aged alloy within 5000 hours was observed.

Although γ' precipitates continue coarsening and volume fraction decreases, there is no obvious decrease of the stress-rupture lifetime during the prolonged thermal exposure between 5000 and 15,000 hours. Based on previous investigation,[30] lattice mismatch appears to be an important factor in the consideration of the influence of γ' particle size on the high temperature creep properties of some alloys. As γ' precipitates are subjected to further coarsening and coalescence, the γ' particles become a more spherical and irregular morphology and semi-coherent or non-coherent, and a higher magnitude of mismatch may result in a finer spacing of misfit dislocations, which in turn would act as a stronger barrier to mobile dislocations.[30] Moreover, the $M_{23}C_6$ precipitates along GB would improve the resistance to GB slip and have a beneficial effect on stress rupture property. Consequently, the stress-rupture lifetime presents no significant change between 5000 and 15,000 hours thermal exposure.

As the thermal exposure was prolonged from 20,000 up to 24,000 hours, GB coarsening facilitated by coarsened γ' layers and severe MC carbides decomposition along GBs took place, which may mainly contribute to

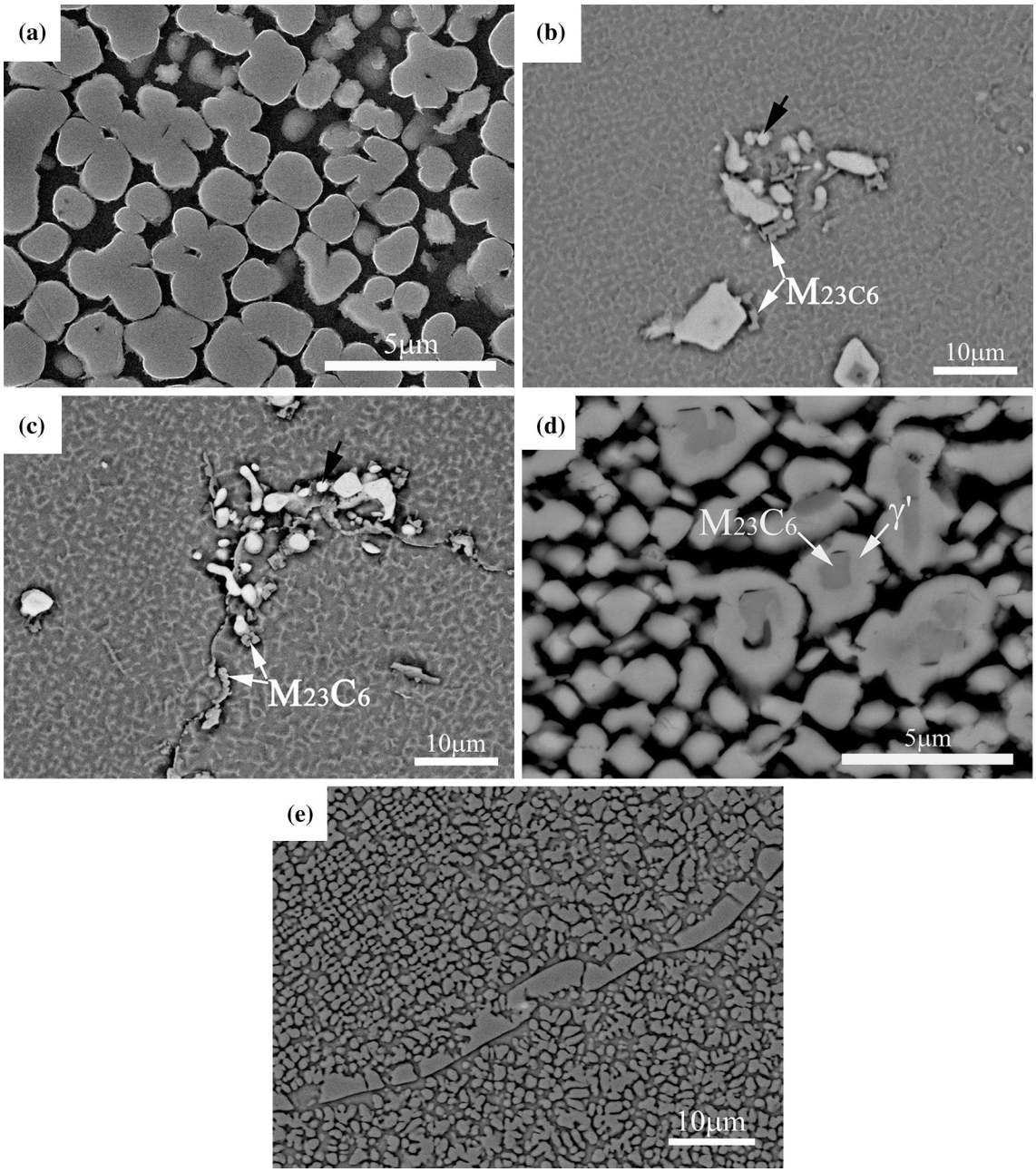

Fig. 6—Microstructure in the thermally exposed alloy for 24,000 h: γ' precipitates (*a*); primary MC carbides within GIs (*b*) and along GBs (*c*); $M_{23}C_6$ particles wrapped by γ' precipitates (*d*); γ' precipitates at grain boundary (*e*).

the secondary decrease of stress-rupture lifetime shown in Figure 10(a). As was reported,[31–33] when the continuous GB structure wrapped by $M_{23}C_6$ and γ' layer severely coarsen, GB is embrittled and become notch sensitive and prone to cracking as illustrated in the fracture (Figures 11(c) and (d)). Although the aim of producing DS superalloy is to eliminate transverse grain boundaries for improving creep properties, GB in the DS superalloys is not completely straight but an approximate linear line with curves. The GB in the curve position performs like a small scale transverse GB during creep. Hence, the coarsened curve grain boundaries after long-term thermal exposure would have significant detrimental effects on the decreasing of stress-rupture lifetime. Consistent with the conclusions in the previous studies,[5,19,20] severe MC decomposition and continuous $M_{23}C_6$ and γ' precipitates near the positions of curve GBs provided the site of cracks initiation and propagation, which reduce the force-bearing area and result in a higher stress level and creep rate, but have not decreased the elongation obviously. Meanwhile, primary MC decomposition within GIs might have no significant influence on stress rupture property of the thermally exposed alloy.

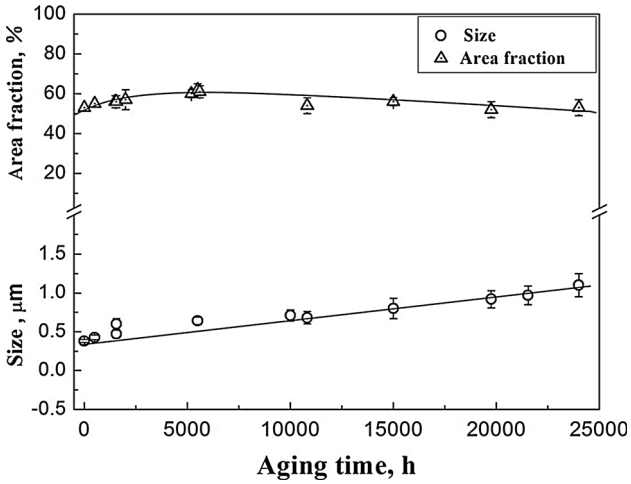

Fig. 7—Evolution of size and area fraction of secondary γ' precipitates during long-term thermal exposure at 1173 K (900 °C).

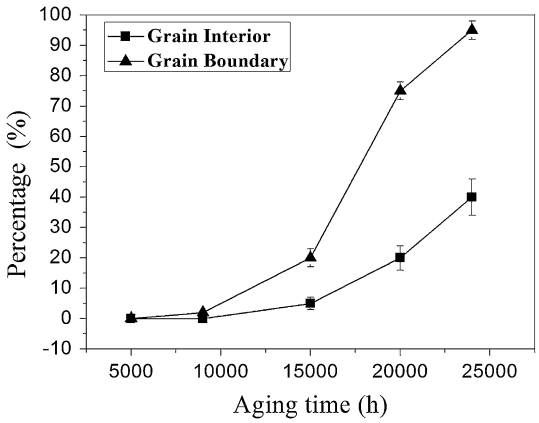

Fig. 8—Variations of the percentage of MC showing disintegration *vs* aging time both within GIs and at GBs.

V. CONCLUSIONS

1. During long-term thermal exposure at 1173 K (900 °C), microstructural degradation of the DS alloy includes γ' coarsening, primary MC decomposition, and GB coarsening. γ' precipitate gradually changed its morphology from cubic to spherical and irregular. The coarsening kinetic appears to conform well to the LSW model during long-term thermal exposure. Primary MC decomposed to a tiny degree and was surrounded by a well-defined decomposition zone within 5000 hours. As the thermal exposure was extended over 9000 hours, primary MC decomposed into $M_{23}C_6$ carbides wrapped by γ', which can be summarized as MC + $\gamma \rightarrow M_{23}C_6 + \gamma'$. As the thermal exposure was prolonged up to 20,000 and 24,000 hours, the MC decomposition proceeded and more decomposed MC broken down into smaller MC-type disintegrated particles. GB coarsening was mainly facilitated by $M_{23}C_6$ carbides and γ' precipitates coarsening in GBs region, and the GB coarsening kinetics conforms well to the JMAK theory.

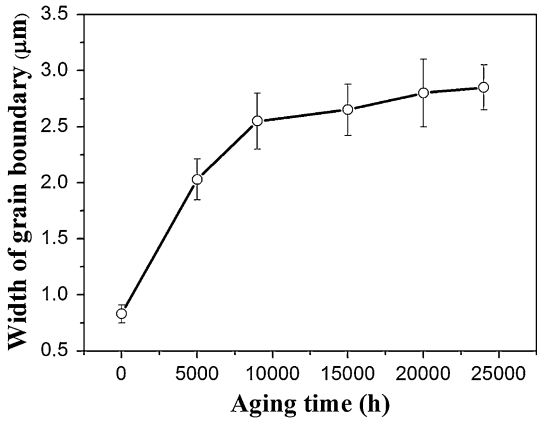

Fig. 9—The width of grain boundaries after thermal exposure at 1173 K (900 °C) for different aging times.

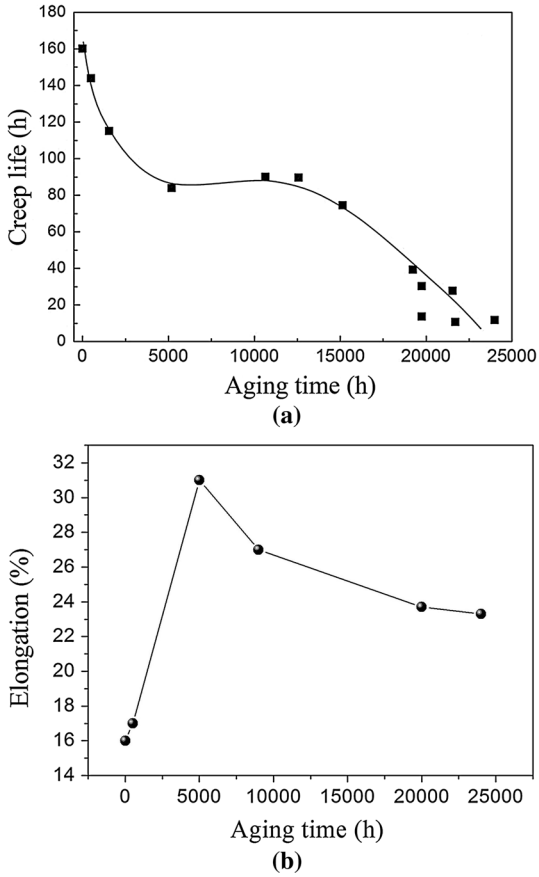

Fig. 10—Stress-rupture lifetime (*a*) and elongation (*b*) of the thermally exposed alloy.

2. The stress-rupture lifetime at 1253 K (980 °C) exhibits three stages during thermal exposure. The stress-rupture lifetime decreases sharply by 50 pct within 5000 hours and then remains at a steady level from 5000 to 15,000 hours. Finally, the lifetime of stress rupture decreases drastically again to about 10 pct of that of the virgin alloy as the thermal exposure time is over 15,000 hours.

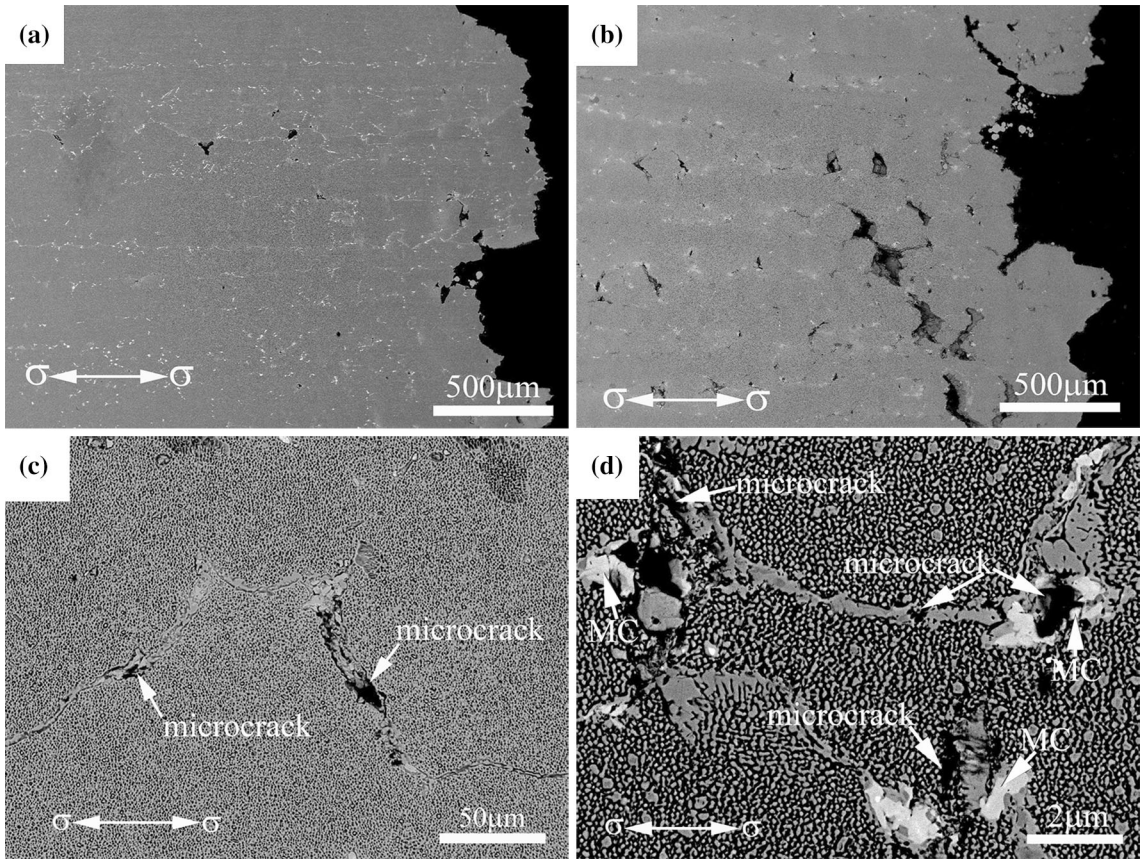

Fig. 11—Backscattered electron (BSE) imaging of longitudinal section near the rupture site in the creep rupture specimens of the thermally exposed alloy for 5000 h (*a*) and 24,000 h (*b*, *c* and *d*).

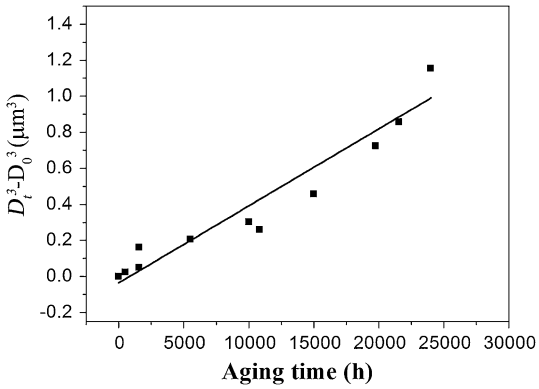

Fig. 12—Variations of $\bar{D}_t^3 - \bar{D}_0^3$ *vs* time for secondary γ' precipitates.

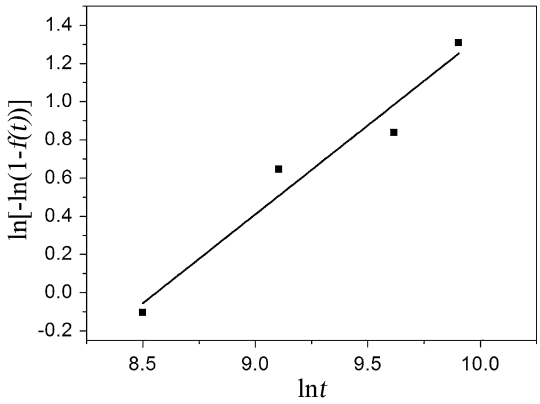

Fig. 13—Variations of ln[−ln(1−*f*(*t*))] *vs* ln*t* during long-term isothermal exposure at 1173 K (900 °C).

3. During different stages of the thermal exposure, dominant factors for the decrease of stress-rupture lifetime vary due to the evolution of multiple microstructures. Secondary γ' coarsening and widening of γ matrix channel facilitate the movement of mobile dislocations, which mainly cause a significant decreasing of stress rupture life of the thermally exposed alloy within 5000 hours. Although γ' coarsening continues between 5000 and 15,000 hours thermal exposure, the γ' particles become a more spherical and irregular morphology and semi-coherent or non-coherent, and a higher magnitude of mismatch may result in a finer spacing of misfit dislocations, which in turn would act as a stronger barrier to mobile dislocations. Moreover, the discrete $M_{23}C_6$ precipitates along GB would improve the resistance to GB slip and have a beneficial effect on stress rupture properties. Due to these effects, the stress-rupture lifetime of the alloy between 5000 and 15,000 hours presents no obvious change. The severe MC decomposition and continuous coars-

ened $M_{23}C_6$ and γ' precipitates at the curve grain boundaries facilitate the initiation and propagation of microcracks after the thermal exposure from 20,000 up to 24,000 hours and result in the drastic drop of the stress rupture life.

ACKNOWLEDGMENTS

Present work were supported by the National "863" Project 2012AA03A511, 2012AA03A513, the National Basic Research Program (973 Program) of China under Grant No. 2010CB631201 and the National Natural Science Foundation of China under Grant No. 51101160, 51171193. The authors are grateful for these supports.

REFERENCES

1. J.C. Chang, Y.H. Yun, and C. Choi: *Eng. Fail. Anal.*, 2003, vol. 10, pp. 559–67.
2. M. Konter and M. Thumann: *J. Mater. Process. Technol.*, 2001, vol. 117, pp. 386–90.
3. E. Lvova and D. Norsworthy: *J. Mater. Eng. Perform.*, 2001, vol. 10, pp. 299–12.
4. E. Lvova: *J. Mater. Eng. Perform.*, 2007, vol. 16, pp. 254–64.
5. G. Lvov, V.I. Levit, and M.J. Kaufman: *Metall. Mater. Trans. A*, 2004, vol. 35A, pp. 1669–79.
6. M. Lifshitz and V.V. Slyozov: *J. Phys. Chem. Solids*, 1961, vol. 19, pp. 35–50.
7. C. Wagner: *Z. Elektrochem.*, 1961, vol. 65, pp. 581–91.
8. D.J. Chellman and A.J. Ardell: *Acta Metall.*, 1974, vol. 22, p. 577.
9. D. McLean: *Met. Sci.*, 1984, vol. 18, p. 249.
10. A.J. Ardell: *Scripta Metall. Mater.*, 1990, vol. 24, p. 343.
11. A. James: *Mater. Sci. Technol.*, 2001, vol. 17, pp. 481–86.
12. L.H. Rettberg, M. Tsunekane, and T.M. Pollock: in *Superalloys 2012*, E.S. Huron, R.C. Reed, M.C. Hardy, M.C. Mills, R.E. Montero, P.D. Portella, and J. Telesman, eds., TMS, Warrendale, PA, 2012, pp. 341–49.
13. S. Pahlavanyali, M. Wood, and G. Marchant: in *Superalloys 2012*, E.S. Huron, R.C. Reed, M.C. Hardy, M.C. Mills, R.E. Montero, P.D. Portella, and J. Telesman, eds., TMS, Warrendale, PA, 2012, pp. 463–71.
14. B.G. Choi: *Mater. Sci. Eng. A*, 2008, vol. 478, pp. 329–35.
15. X.B. Huang, Y. Kang, H.H. Zhou, Y. Zhang, and Z.Q. Hu: *Mater. Lett.*, 1998, vol. 36, p. 210.
16. L.Z. He, Q. Zheng, X.F. Sun, H.R. Guan, Z.Q. Hu, A.K. Tieu, C. Lu, and H.T. Zhu: *Mater. Sci. Eng. A*, 2005, vol. 397, pp. 297–04.
17. L.Z. He, Q. Zheng, X.F. Sun, G.C. Hou, H.R. Guan, and Z.Q. Hu: *J. Mater. Sci.*, 2005, vol. 40, p. 2959.
18. Q.Z. Chen, C.N. Jones, and D.M. Knowles: *Mater. Sci. Eng. A*, 2004, vol. 385, pp. 402–18.
19. X.Z. Qin, J.T. Guo, C. Yuan, C.L. Chen, and H.Q. Ye: *Metall. Mater. Trans. A*, 2007, vol. 38A, pp. 3014–22.
20. L.R. Liu, T. Jin, N.R. Zhao, Z.H. Wang, X.F. Sun, H.R. Guan, and Z.Q. Hu: *Mater. Sci. Eng. A*, 2003, vol. 361, p. 191.
21. E.W. Ross and C.T. SIMS: in *Superalloy II*, C.T. SIMS, N.S. Stoloff, and W.C. Hagel, eds., Wiley, New York, 1987, pp. 97–134.
22. Q. Zeng, P. Yan, C. Shao, J.C. Zhao, F.K. Han, and L.F. Zhang: *Acta Metall. Sin.*, 2013, vol. 49, pp. 63–70.
23. J.W. Cahn: *Acta Metall.*, 1956, vol. 4, p. 449.
24. M.C. Weinberg, D.P. Birnie, III, and V.A. Shneidman: *J. Non-Cryst. Solids*, 1997, vol. 219, pp. 89–99.
25. J.W. Christian: *The Theory of Transformations in Metals and Alloys*, 2nd ed., Pregamon, Kidlington, 2002.
26. G.S. Ansell and J. Weertman: *Trans. Metall. Soc. AIME*, 1956, vol. 215, pp. 838–43.
27. R.C. Reed: *The Superalloys, Fundamentals and Applications*, Cambridge University Press, Cambridge, 2006.
28. R.A. Stevens and P.E.J. Flewitt: *Mater. Sci. Eng.*, 1979, vol. 37, pp. 237–47.
29. M. Aghaie-Khafri and M. Hajjavady: *Mater. Sci. Eng. A*, 2008, vol. 487, pp. 388–93.
30. M.V. Nathal: *Metall. Trans. A*, 1987, vol. 18A, pp. 1961–70.
31. A.K. Koul and R. Castillo: *Metall. Mater. Trans. A*, 1988, vol. 19A, p. 2049.
32. C.T. Sims, N.S. Stoloff, and W.C. Hagel: *Superalloy*, Wiley, New York, NY, 1987.
33. A.G. Mohammad and M. Mohsen: *Mater. Des.*, 2011, vol. 32, pp. 2695–2700.